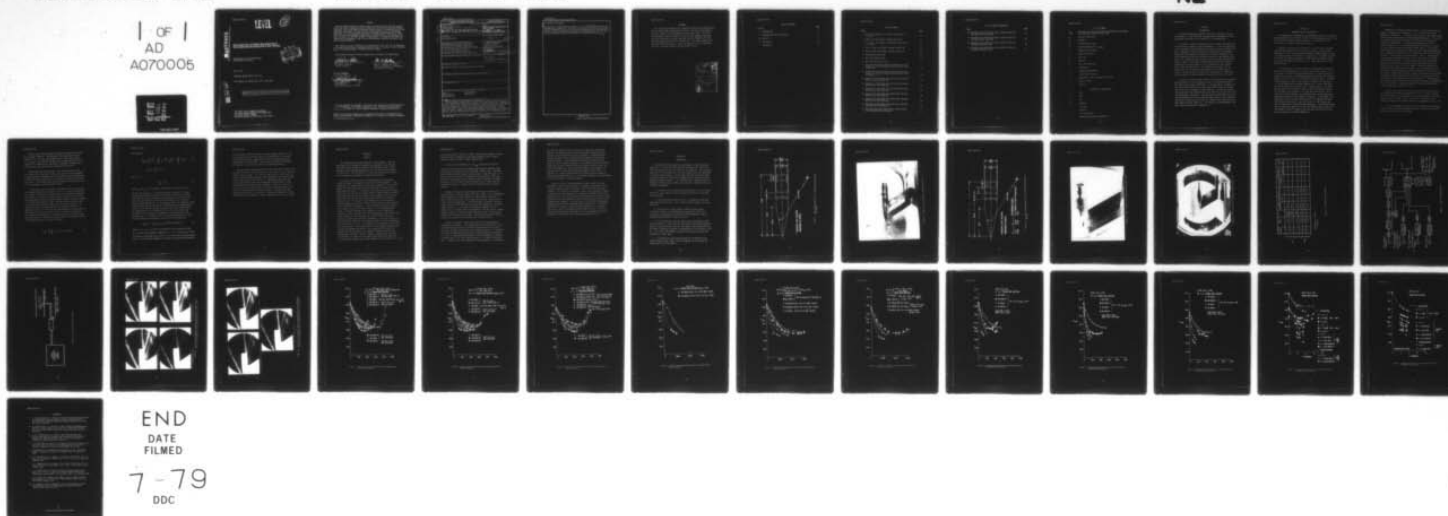AD-A070 005   AIR FORCE FLIGHT DYNAMICS LAB WRIGHT-PATTERSON AFB OH   F/G 19/4
GAU-8 PROJECTILE AFTERBODY DRAG REDUCTION BY BOATTAILING AND BA--ETC(U)
APR 79   W CALARESE

UNCLASSIFIED   AFFDL-TR-78-161   NL

| OF |
AD
A070005

END
DATE
FILMED

7-79
DDC

AFFDL-TR-78-161

LEVEL

GAU-8 PROJECTILE AFTERBODY DRAG REDUCTION BY
BOATTAILING AND BASE INJECTION WITH HEAT ADDITION

Aerodynamics and Airframe Branch
Aeromechanics Division

April 1979

TECHNICAL REPORT AFFDL-TR-78-161

Final Report for Period July 1977 - May 1978

Approved for public release; distribution unlimited.

AIR FORCE FLIGHT DYNAMICS LABORATORY
AIR FORCE WRIGHT AERONAUTICAL LABORATORIES
AIR FORCE SYSTEMS COMMAND
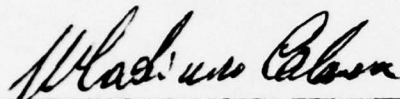WRIGHT-PATTERSON AIR FORCE BASE, OHIO 45433

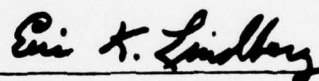This technical report has been reviewed and is approved for publication.
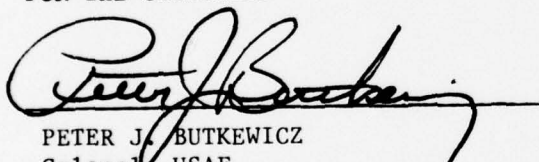

WLADIMIRO CALARESE
Project Engineer

ERIC K. LINDBERG, Maj, USAF
Chief, Aerodynamics & Airframe Br.
Aeromechanics Division

FOR THE COMMANDER

PETER J. BUTKEWICZ
Colonel, USAF
Chief, Aeromechanics Division

AIR FORCE/56780/7 May 1979 — 225

SECURITY CLASSIFICATION OF THIS PAGE (When Data Entered)

REPORT DOCUMENTATION PAGE		READ INSTRUCTIONS BEFORE COMPLETING FORM
1. REPORT NUMBER AFFDL-TR-78-161	2. GOVT ACCESSION NO.	3. RECIPIENT'S CATALOG NUMBER
4. TITLE (and Subtitle) GAU-8 PROJECTILE AFTERBODY DRAG REDUCTION BY BOATTAILING AND BASE INJECTION WITH HEAT ADDITION		5. TYPE OF REPORT & PERIOD COVERED Final Report July 1977 - May 1978
		6. PERFORMING ORG. REPORT NUMBER
7. AUTHOR(s) Wladimiro Calarese		8. CONTRACT OR GRANT NUMBER(s)
9. PERFORMING ORGANIZATION NAME AND ADDRESS Aerodynamics and Airframe Branch (FXM) Air Force Flight Dynamics Laboratory Wright-Patterson Air Force Base, Ohio 45433		10. PROGRAM ELEMENT, PROJECT, TASK AREA & WORK UNIT NUMBERS Project No. 1929 Task No. 192950 Work Unit No. 19295001
11. CONTROLLING OFFICE NAME AND ADDRESS Air Force Flight Dynamics Laboratory Wright-Patterson Air Force Base, Ohio 45433		12. REPORT DATE April 1979
		13. NUMBER OF PAGES 41
14. MONITORING AGENCY NAME & ADDRESS(if different from Controlling Office)		15. SECURITY CLASS. (of this report) Unclassified
		15a. DECLASSIFICATION/DOWNGRADING SCHEDULE

16. DISTRIBUTION STATEMENT (of this Report)

Approved for public release; distribution unlimited

17. DISTRIBUTION STATEMENT (of the abstract entered in Block 20, if different from Report)

18. SUPPLEMENTARY NOTES

19. KEY WORDS (Continue on reverse side if necessary and identify by block number)

Drag	Base Injection
Drag reduction	Boattailing
Afterbody drag	

20. ABSTRACT (Continue on reverse side if necessary and identify by block number)

An experimental investigation was performed on a GAU-8 mm projectile model in order to determine whether base injection of different gases at a temperature of up to 900°R, which simulates the effects of fumers, would produce a reduction in the afterbody drag. Wind tunnel tests were performed at Mach 3, using different boattail angles and two different gases, air and helium. Pressure data were taken, together with schlieren photographs illustrating the flow field. Results show that afterbody drag reduction of 30% to 40% is obtained by small

DD FORM 1473 EDITION OF 1 NOV 65 IS OBSOLETE
1 JAN 73

SECURITY CLASSIFICATION OF THIS PAGE (When Data Entered)

012 070

20. Abstract (Continued)

gas injection. Afterbody boattail angles of 4° to 7° *angles* additionally reduce the afterbody drag by about 15%. Injection of gas heated to 700°R does not further reduce the afterbody drag but increasing the temperature of the injected gas up to 900°R produces an afterbody drag reduction of approximately 15%. For the same mass injection rates, helium injection is more efficient than air.

FOREWORD

This report was prepared by Dr. Wladimiro Calarese of the Applications
Analysis Group (FXM), Aeromechanics Division, Air Force Flight Dynamics
Laboratory (AFFDL), Wright-Patterson Air Force Base, Ohio. The study
was performed in-house in support of the Air Force Armament Laboratory,
Eglin Air Force Base, Florida, under Work Unit No. 19295001 and covers
work performed between July 1977 and May 1978. The author expresses his
gratitude to Messrs. Norman E. Scaggs and Howard L. White of the AFFDL
for their contribution during the wind tunnel testing.

TABLE OF CONTENTS

LIST OF FIGURES

LIST OF FIGURES (CONTINUED)

LIST OF SYMBOLS

$C_{D_{AB}}$	Afterbody Drag Coefficient Based on Maximum Cross-Sectional Area (does not include rifling ring)
C_p	Pressure Coefficient
D	*Diameter*
FR	Fineness Ratio, L/D_M
I	Mass Flow Parameter, $\dot{m}/\rho_\infty u_\infty S_M$
ℓ	Boattail Axial Length
L	Model Axial Length
$\dot{m}$	Mass Flow
p	Pressure
S	Cross-Sectional Area
T	Temperature
T_o	Stagnation Temperature
u	Longitudinal Velocity
x	Coordinate in the Longitudinal Direction
β	Boattail Angle
ρ	Density

SUBSCRIPTS & SUPERSCRIPTS

b	Base
g	Gas
$\dot{j}$	Jet
M	Maximum
∞	Infinity
β	Boattail
'	First Derivative
-	Nondimensionalized with Respect to ℓ

SECTION I

INTRODUCTION

The high afterbody drag penalties incurred in supersonic flow by slender bodies of revolution have stimulated many investigators to find some methods that might give a reduction in the afterbody drag.

An attempt to reduce the afterbody drag of a GAU-8 30 mm projectile was first made by Freeman & Korkegi (Reference 1). They used boattailing of the afterbody and base blowing of cold gases to reduce the projectile drag. Subsequently Calarese and Walterick (Reference 2) performed an experimental investigation to optimize the results of Reference 1 and used a combination of boattail and base injection of gases heated up to 700°R. This combination did not improve the results obtained with base injection alone. The present investigation treats the base injection problem with particular emphasis on the temperature of the injected gases, which now attain 900°R. The injection of hot gases (air and helium) was used to simulate fumer elements, such as those used in tracers. One of the two gases used, air, was selected to simulate the molecular weight of typical products of combustion, which is 20 to 25.

In order to find the optimum condition for minimum drag, a trade-off between boattail and base drag must be used. Base pressure problems have been studied by many (Reference 3). The base drag is generated by the low pressure created by the shear layer that separates at the base corner and usually undergoes a strong expansion. In order to increase the base pressure and reduce the drag, gas injection has been used in the past (References 4 through 8). Many parameters contribute to the value of the afterbody drag; such as injection rate, boattail angle, injection temperature, type of gas or gas mixture, boundary layer characteristics, Mach number, Reynolds number, etc. The effects of these parameters have been extensively analyzed in Reference 2.

1

SECTION II

EQUIPMENT AND TEST DESCRIPTION

The experiment was performed at two different wind tunnels, the High Reynolds Number Facility (HiReF) and the Trisonic Gasdynamics Facility (TGF) of the Air Force Flight Dynamics Laboratory. A description of the facilities can be found in References 9 and 10.

The Mach 3 wind tunnel of the HiReF is a 2-D cold flow, blow down type wind tunnel with an 8 by 8.2 inch test section. The tests were conducted on a full size strut mounted projectile model (Figures 1 and 2) illustrated in detail in Reference 7, at Mach 2.93, a stagnation pressure of 75 psia and a Reynolds number of 8×10^6 based on the model length. The projectile fineness ratio (FR) is 5.15. Base injection of air and helium was used.

The TGF consists of a closed circuit 2-D wind tunnel for subsonic, transonic, and supersonic flow. The size of the test section is 23.7 by 23.7 inches. The tests were conducted at Mach 3, a tunnel stagnation pressure of 24.3 psia, a stagnation temperature of 550°R, and a Reynolds number of 4.8×10^6 and 5.3×10^6 based on the model lengths. The model is approximately 2.8 times scale version of a GAU-8 30 mm. projectile. It is strut mounted with a maximum diameter of 3.47 inches (excluding the rifling ring), two different overall lengths, one of 17.60 inches, and the other of 15.89 inches in order to obtain two fineness ratios, one the same as the projectile, 5.15, and the other smaller, 4.64, to alter the turbulent boundary layer characteristics without appreciably affecting the external flow (Figures 3 through 5). In Reference 2 two models were tested, the full scale model of 5.15 fineness ratio with cold injection, and the 2.8 times scale model of 4.64 fineness ratio with gas injection of 520°R and 700°R temperature. In the present study the 2.8 times scale model of 4.64 and 5.15 fineness ratio and the full scale model of the 5.15 fineness ratio have been tested with cold and hot gas injection up to 900°R temperature.

2

AFFDL-TR-78-161

Afterbodies of different boattail angles, β, were tested (Figure 6), however, the emphasis was placed on $\beta = 4°$ to $7°$ due to the results presented in Reference 2. The shape and the caliber of the boattails were selected after consultation with the AF Armament Laboratory. The conical 1/2 caliber boattails were selected due to stability and projectile fabrication requirements. The models were equipped with 10 to 13 static pressure taps, 1 or 2 ahead and behind the rifling ring located in the 0° meridian plane of the model and 180° apart; 4 to 6 pressure taps located on the boattails 15° apart from each other peripherally and 2 to 3 pressure taps were located in the base area, flush with the model in the 0° - 180° meridian plane (see Figures 1 and 3). The average of the base pressure readings was used since in most cases the readings were virtually identical. In addition two high response transducers were also used in the TGF to measure dynamic pressures, one on the boattail and the other in the base region. They were referenced to a variable pressure system which was manually set and recorded for each test point. Voltage readouts from the transducers were fed directly to the TGF mini computer where dynamic pressure coefficients were calculated. The model pressure transducers were connected to the computer for the calculation of the afterbody pressure drag (Figure 7). A thermocouple was installed inside the model settling chamber to measure the temperature of the injected gas. The maximum injection temperature attained was 1100°R in the HiReF and 900°R in the TGF.

The bases consisted of 5 to 6 micron porous metal disks used for base injection with injection diameters of 1.44, 1.75, and 1.8 inches for the TGF model which correspond to an injection diameter to maximum diameter ratio of $D_j/D_M = 0.42$, 0.51, and 0.52, respectively, and 0.62 inch diameter for the HiReF model which corresponds to $D_j/D_M = 0.52$.

The strut's sweepback angle was 60°, the leading and trailing half angles, 8.64° each, and the maximum thickness, 0.25 inch for the HiReF model and 0.72 inch for the TGF model.

3

The mass flow system provided the secondary flow for cold and hot gas injection (Figure 8). The secondary flow was measured using a choked orifice. The mass flow parameter used in the present study, $I = \dot{m}/\rho_\infty u_\infty S_M$, is the ratio of the mass flow injected and the mass flow captured by a stream tube of area equal to the model's maximum cross-sectional area, S_M, which does not include the rifling ring.

Experimental data were obtained in both the HiReF and the TGF. In this manner, full scale and 2.8 times scale results could be compared. The same proportions between tunnel size and model size were maintained in both facilities to ascertain if different wind tunnels would affect the results. The afterbody drag values obtained were plotted versus the mass flow parameter I and the boattail angle β.

The flow field over the projectile afterbody can be clearly seen in the schlieren photographs of Figures 9 and 10. It can be observed that the increase in base injection rates changes the near wake considerably and produces an opening in the wake throat. The expansion at the base corner decreases and the base pressure becomes higher. Further increases in injection rates produce a shock at the base corner signifying that the base pressure has become higher than the boattail pressure. The corner shock losses are more than offset by the base pressure rise. Additional increases in injection rates add momentum to the wake and the entrainment action begins causing an early closure of the near wake. The afterbody drag decreases at the beginning for small injection rates but then reverses its trend and increases because of entrainment losses. The afterbody drag was calculated as follows:

$$C_{D_{AB}} = \frac{1}{S_M} \int_0^\ell C_{p_\beta} \, S'dx - C_{p_b} \, S_b/S_M \tag{1}$$

4

which becomes

$$
C_{D_{AB}} = \frac{8}{\bar{D}_M^2} \tan^2 \beta \int_0^1 C_{p_\beta} \bar{x} d\bar{x} - \frac{4}{\bar{D}_M} \tan \beta \int_0^1 C_{p_\beta} d\bar{x} \qquad (2)
$$

$$
- C_{p_b} (1 - \frac{2}{\bar{D}_M} \tan \beta)^2
$$

and for $\beta = 0°$

$$
C_{D_{AB}} = -C_{p_b} \qquad (3)
$$

where C_{p_β} and C_{p_b} are respectively the pressure coefficients of the boattail and the base, β is the boattail angle, and $\bar{D}_M$ is the maximum body diameter nondimensionalized with respect to the boattail length. Some difficulties were encountered during the tests in the HiReF (blow down type) with regard to pressure values obtained at low injection rates and high temperatures. At low injection rates, the temperature drop of the injected gas was very rapid. Starting with a gas temperature of 1000°R, by the time the readings were taken after the transient period the temperature was too low (about 750°R) to be of any significance. To have an idea of how much the temperature values would affect the base pressure, it is useful to show a correlation (Reference 6) of base pressure changes with temperature increases of the injected gas

$$
p_{base}/p_\infty = (P_{base}/P_\infty)_{I=0} + (12.25 + 0.002778\Delta T) \, I \qquad (4)
$$

where $\Delta T = T_g - T_{o_\infty}$, T_g being the temperature of the injected gas and T_{o_∞} the freestream stagnation temperature. If ΔT is of the order of 200°R, the change in afterbody drag is only 1% to 2%, well within the experimental error. It is necessary therefore to increase the injected gas temperature

5

to approximately 1000°R to obtain a sizeable change of about 8% to 10%. It was necessary then to heat the gas to be injected to a much higher than needed temperature, approximately 1200°R, to achieve injection temperatures of at least 900°R. Very careful monitoring of the heater was required to check for hot spots which might have burned it.

Another problem encountered was due to the long time it took for the pressure transducers to become stable after the tunnel start, so that the readings could be taken. This time lag, about 30 secs., was due to the large pressure difference between tunnel atmospheric values at the start and low local pressure levels at $M_\infty \simeq 3$, and produced very high heat losses, lowering the injected gas temperature to below 800°R. It was then decided to keep the pressure transducers closed for the first 10 to 15 secs. after the tunnel start (at almost vacuum conditions) to let the flow settle and avoid the transient period. Then the lines were opened and the pressure taps reached a steady value immediately so that the readings could be taken at a higher temperature, at least $T_g = 900°R$.

SECTION III

RESULTS

No unsteady pressures were detected on the TGF models. The root mean square of the pressure fluctuations was obtained in the TGF using the high response transducers located in the afterbody region. When divided by the freestream dynamic pressure, its value was of the order of 10^{-3} to 10^{-4}. For the TGF this is a very low value within the noise level, indicating the presence of steady flow conditions.

For the air injection case, the afterbody drag coefficient was plotted in Figures 11 through 13 versus the mass flow parameter I. The present data are compared with previous data of Reference 2 to ascertain whether different wind tunnels and different model's fineness ratios would affect the results. In addition, the present data show the effects produced by the injection in the base region of gases heated up to 900°R. Small rates of mass injection through the base produce at first a drag coefficient reduction but the trend reverses itself with increasing injection rates. The increase of the temperature of the injected air from room temperature, 520°R, to 700°R did not produce any drag reduction in the experiment of Reference 2. The difference in the model fineness ratio produced only a small change, about 5%, in the afterbody drag levels. The higher FR model, which represents a more slender body, yielded less drag. The data of the present experiment, where the injected air was heated to 900°R, show that for a given injection rate drag reduction increases with increasing temperature. The curve of Figure 11 for the HiReF air injection, for a boattail angle of 4° and a temperature of 900°R, branches out at I = 0.01 because of a malfunction of one of the base pressure taps. In this particular case the readings of the two base taps were considerably different. Since averaging of the different readings was not advisable, it was decided to show both results, not knowing which reading was correct. However, comparing this curve with all the others, it seems that the lower branch might be the right one. The maximum drag reduction due to heat addition is of the order of 10% to 15%.

The 5° angle boattail, Figure 12, seems to be the most effective in drag reduction since it produces the same drag reduction as the 7° angle boattail, Figure 13, but at a lower injection rate.

In Figure 13 the difference in the $C_{D_{AB}}$ values for the cold air injection is mainly due to the different base injection diameter used, with some small effects due to the different fineness ratio. The 900°R injection data from both tunnels are consistent. From these plots it is easy to notice that there is no appreciable tunnel effect. There are three basic drag levels, for any injection rate, observable in Figures 11 through 13; 1.) High drag for low FR and small D_j; 2.) Lower drag for high FR and large D_j; 3.) Lowest drag for high FR, large D_j, and heat addition.

Figures 14 through 16 show the drag coefficient variation due to helium injection. The same trend as for air is seen, i.e., a considerable drag reduction due to small injection, a drag increase (reversal) at higher injection rates and for the same injection rate, lower drag for higher injection temperatures. One more feature is detected: the drag curves for cold helium injection are appreciably different for different fineness ratios, i.e., the lower drag curves are obtained for the higher FR (it is believed that this phenomenon is due not only to a better pressure recovery on the more slender body but also to a better mixing between the helium and the air flow). Data with 900°R helium injection could not be obtained in the TGF because of a heater failure.

Figures 17 through 19 compare the effects of air and helium on afterbody drag reduction. It is evident that hot helium injection gives a better drag reduction than cold helium injection and that, for the same mass injection rate, helium is more effective than air. If Figures 9 and 10 are re-examined keeping in mind the effectiveness of the helium, it is easy to understand the difference in the shock pattern in the wake of the two gases. For mass injection rates of I = 0.006 for the helium and I = 0.0075 for air, close enough rates for comparison, it is observed

8

that the base pressure with air injection is lower than the boattail
pressure. An expansion then occurs at the boattail separation corner.
The base pressure with helium injection, however, is higher than the
boattail pressure, since a quite strong shock emanates from the base
separation corner. Since the boattail pressures are equal for both
gases for lack of upstream influence, it is evident that helium injection
pressurizes the base region more than air injection, which results in a
better drag reduction. This helium effectiveness is attributed to its
lighter molecular weight which produces a higher speed of sound. In
addition, for a given injection rate the volumetric flow of helium is
more than three times that of air. This higher volumetric flow contributes
to the fast increase in the base pressure.

Figures 20 and 21 show how the boattail angle affects the drag
coefficient. At first the increase in β produces a drag reduction but
a further increase produces a reversal in the drag curves and a drag
increase. This reversal is physically correct. For low boattail angles,
as mentioned, the small expansion on the boattail shoulder which causes
boattail drag is more than offset by the base pressure rise due to a lower
expansion at the base separation corner so that the overall effect is an
afterbody drag reduction. For higher angles the boattail drag becomes
predominant and the total afterbody drag increases again. The boattail
angle effect is similar to the mass injection effect. For injection
rates up to $I=0.01$, the optimum condition seems to be at $\beta=7°$ for air
and helium injection with heat addition, with the exception of hot air
injection in the HiReF for which the optimum condition is $\beta=5°$.

AFFDL-TR-78-161

SECTION IV

CONCLUSIONS

An experimental investigation was performed on a GAU-8 projectile model at $M_\infty \sim 3$ to obtain the best possible afterbody drag coefficient reduction by means of base injection with heat addition. Air and helium were used in the investigation. The hot injection tests were performed to simulate fumer elements. Through model modifications and improved testing techniques the injected gas temperature was increased to 900°R producing favorable results. It is possible that a further increase in temperature might produce a higher drag reduction. Additional tests are therefore recommended.

1. A reduction of the afterbody drag coefficient of up to 30% was obtained by small amounts of base injection of air and up to 40% when helium was used.

2. Afterbody boattail angles of 4° to 7° produced an additional drag reduction of about 15%. The 7° angle boattails appear to be more efficient.

3. The injection of gases heated to 700°R did not produce significant changes in the afterbody drag coefficient values, but increasing the temperature of the gases to 900°R produced a further afterbody drag reduction of about 15% to 20%.

4. For the same mass injection rates, helium injection was more efficient than air. This result was attributed to the lighter molecular weight of the helium which increases the speed of sound through the gas and gives a volumetric flow which is approximately 3.5 times that of the air. This larger flow produces a greater base pressure increase and consequently a lower drag.

5. The lower drag levels were obtained for the model with the higher fineness ratio, larger injection diameter, and by heating the injected gas to at least 900°R.
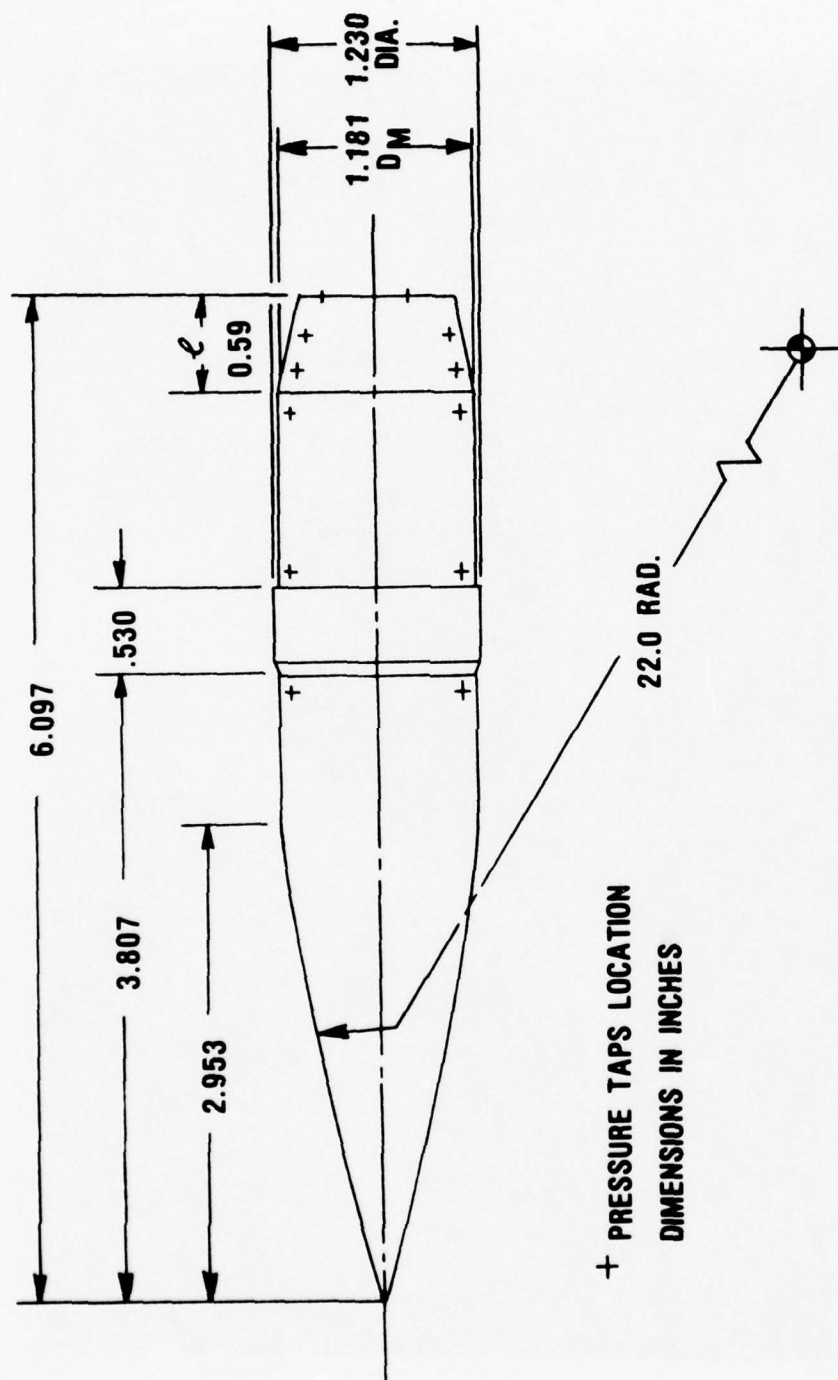
10

1.230 DIA.

1.181 D_M

0.59 ℓ

6.097

.530

3.807

2.953

22.0 RAD.

+ **PRESSURE TAPS LOCATION**

DIMENSIONS IN INCHES

Figure 1. Full Scale Drawing, 5.15 Fineness Ratio Used in the HiReF
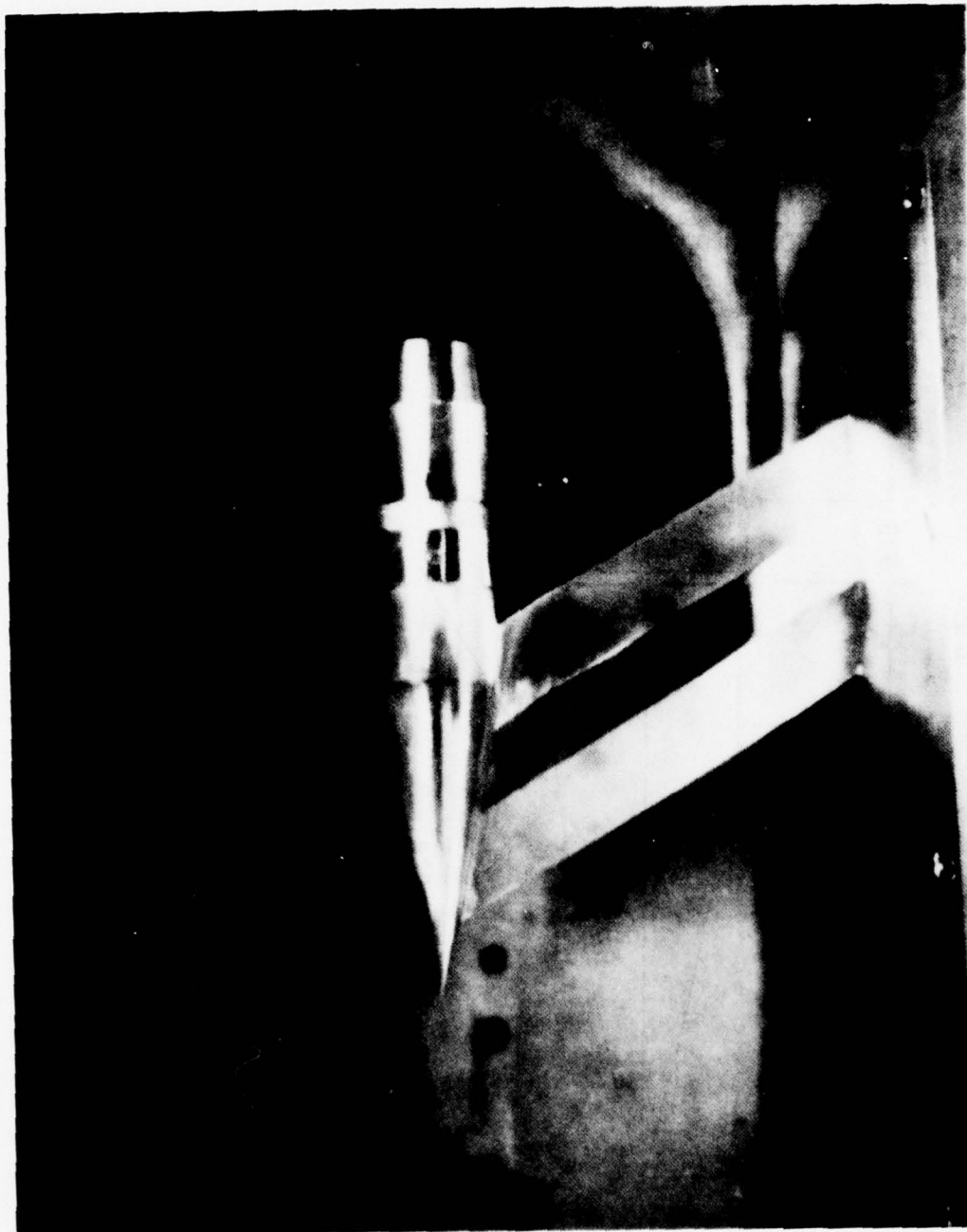
Figure 2. HiReF Full Scale Model, Fineness Ratio 5.15

+ PRESSURE TAPS LOCATION
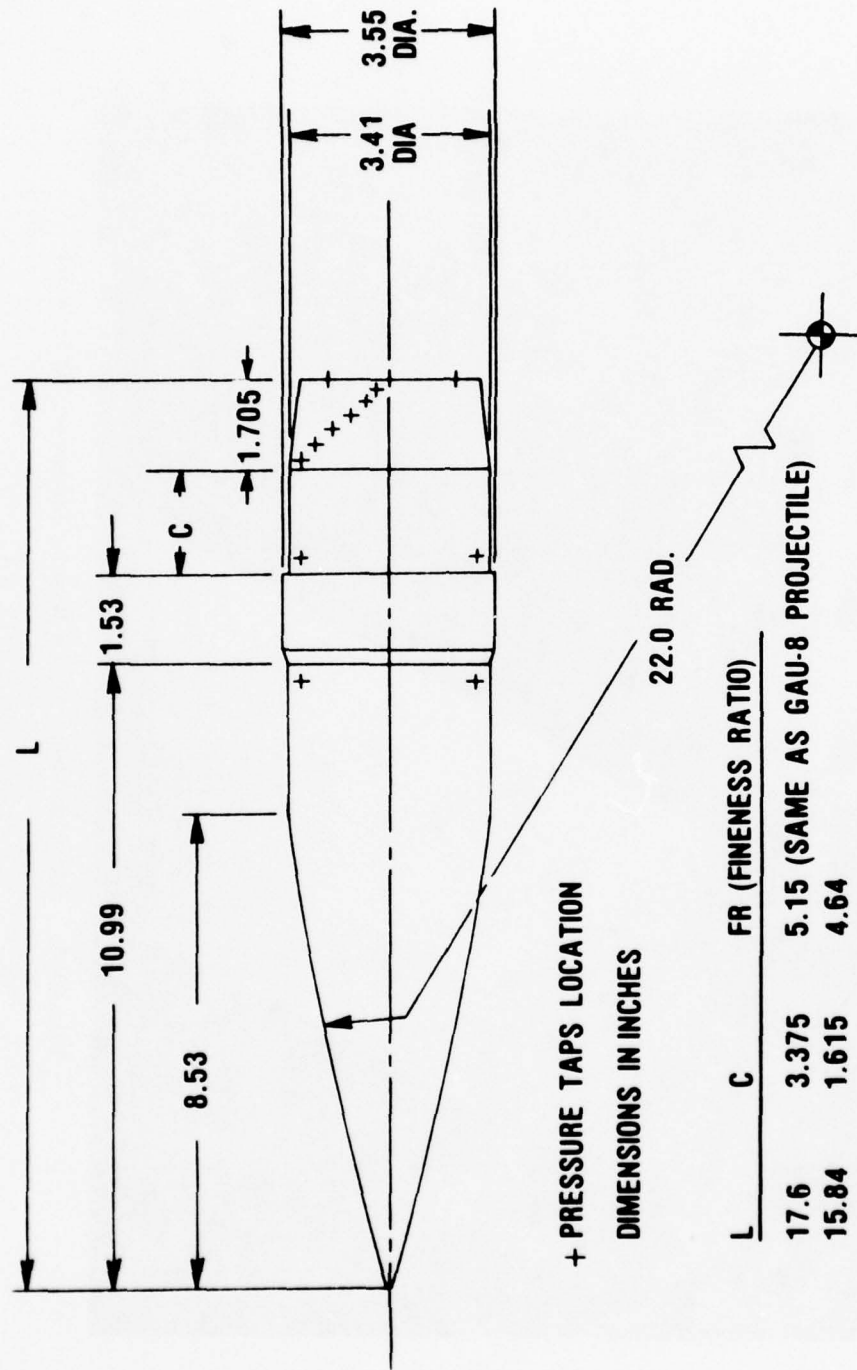
DIMENSIONS IN INCHES

L	C	FR (FINENESS RATIO)	
17.6	3.375	5.15 (SAME AS GAU-8 PROJECTILE)	
15.84	1.615	4.64	

Figure 3. 2.8 Times Scale Drawing, 4.64 Fineness Ratio Used in the TGF
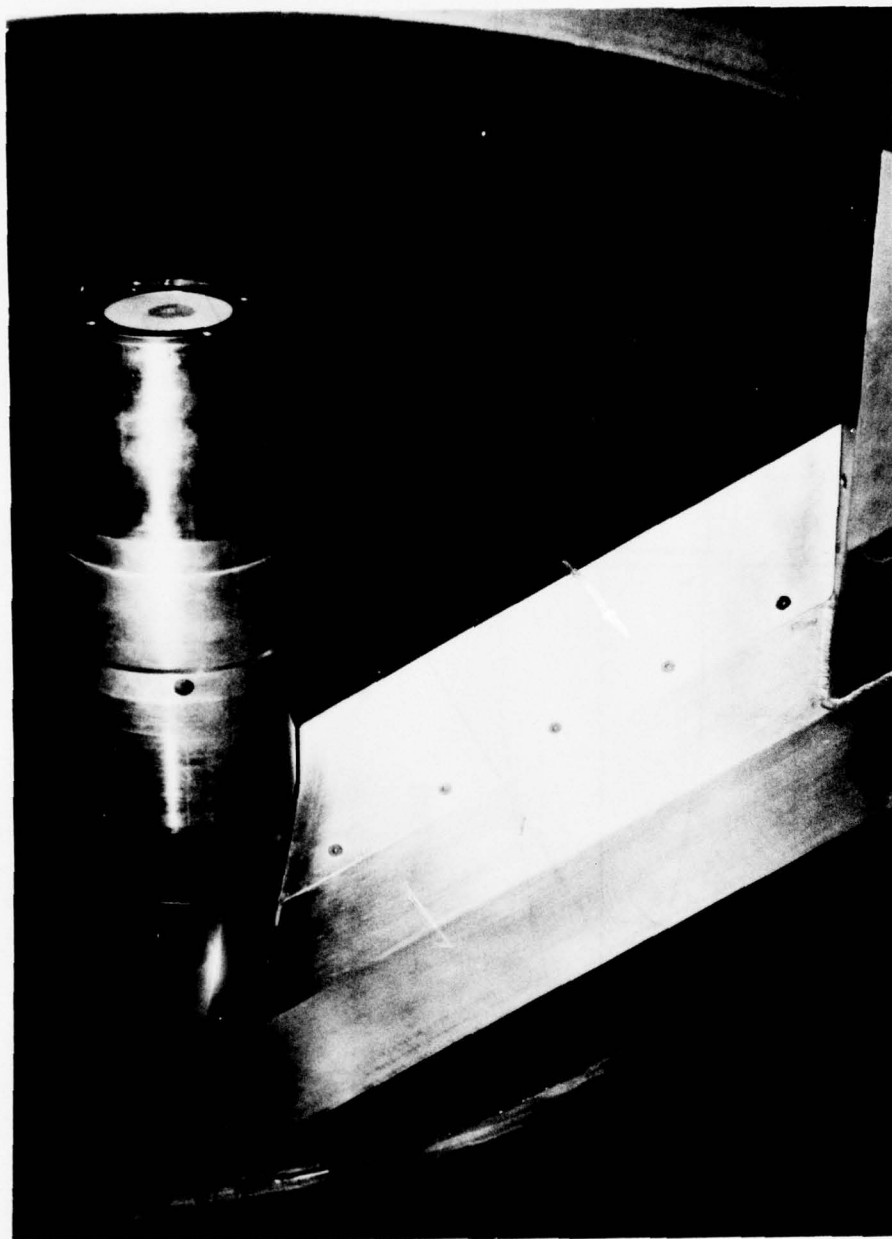
Figure 4. TGF 2.8 Times Scale Model, Fineness Ratio 4.64

Figure 5. TGF 2.8 Times Scale Model, Fineness Ratio 5.15

Cone Angle	Base Diam.*	FR	Base Injection			Pressure		
			Method	Hole Size	Diam*	Hi Response Transducer	Taps on Boattail	Taps in Base
4°	3.172	$\frac{4.64}{5.15}$	Porous	5μ	1.8	0	6	2
5°	3.113	$\frac{4.64}{5.15}$	Porous	5μ	1.8	2	6	3
7°	2.993	$\frac{4.64}{5.15}$	Porous	5μ	1.75	0	6	2
4°	1.098	5.15	Porous	6μ	0.62	0	4	2
5°	1.078	5.15	Porous	6μ	0.62	0	4	2
7°	1.036	5.15	Porous	6μ	0.62	0	4	2

TGF (first three rows), HiReF (last three rows)

*Dimensions in Inches

μ = microns

Figure 6. Afterbody Configurations

16
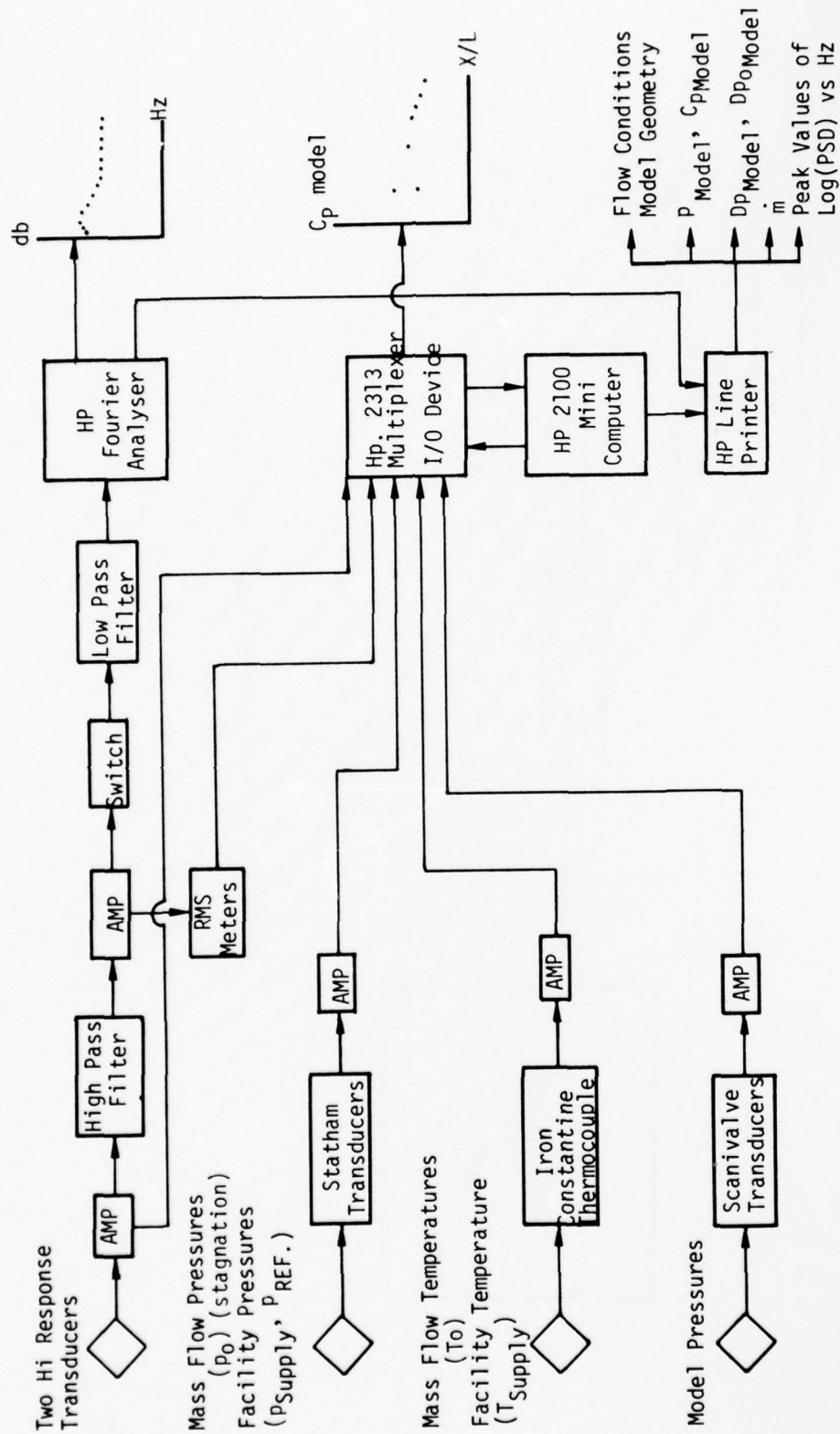
Figure 7. Data Flow Diagram (TGF)

17
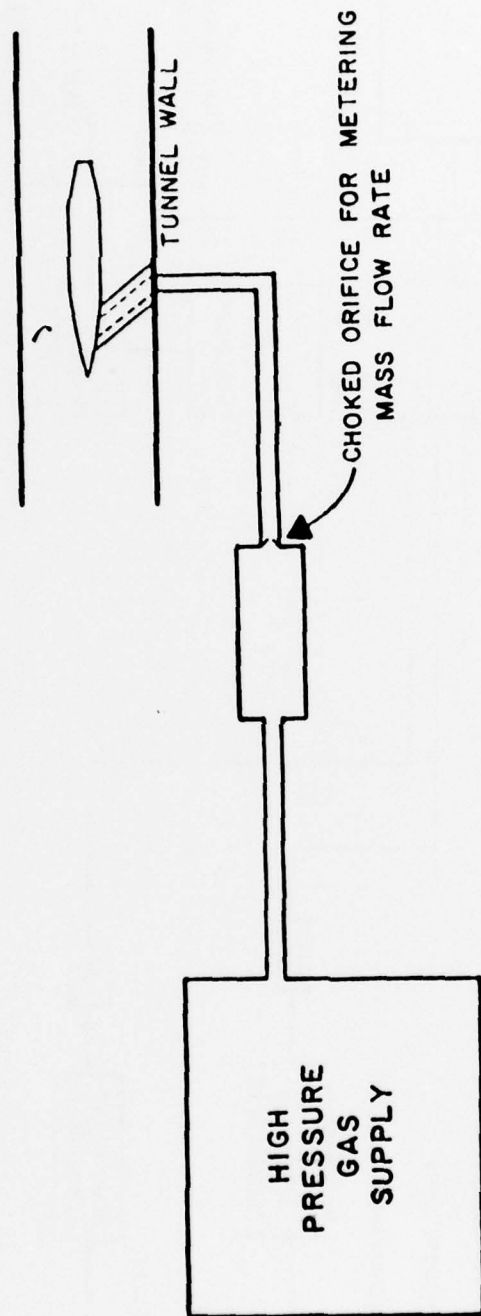
Figure 8. Base Injection Flow System

b. I=0.01, Tg=850°R

d. I=0.022, Tg=925°R

a. I=0.0075, Tg=815°R

c. I=0.015, Tg=830°R

Figure 9. Schlieren Photographs Showing Afterbody Flow Field Changes
Due to the Increase of Base Injection Rates of Air; β=7°

19

a. I-0.0036, Tg=830°R
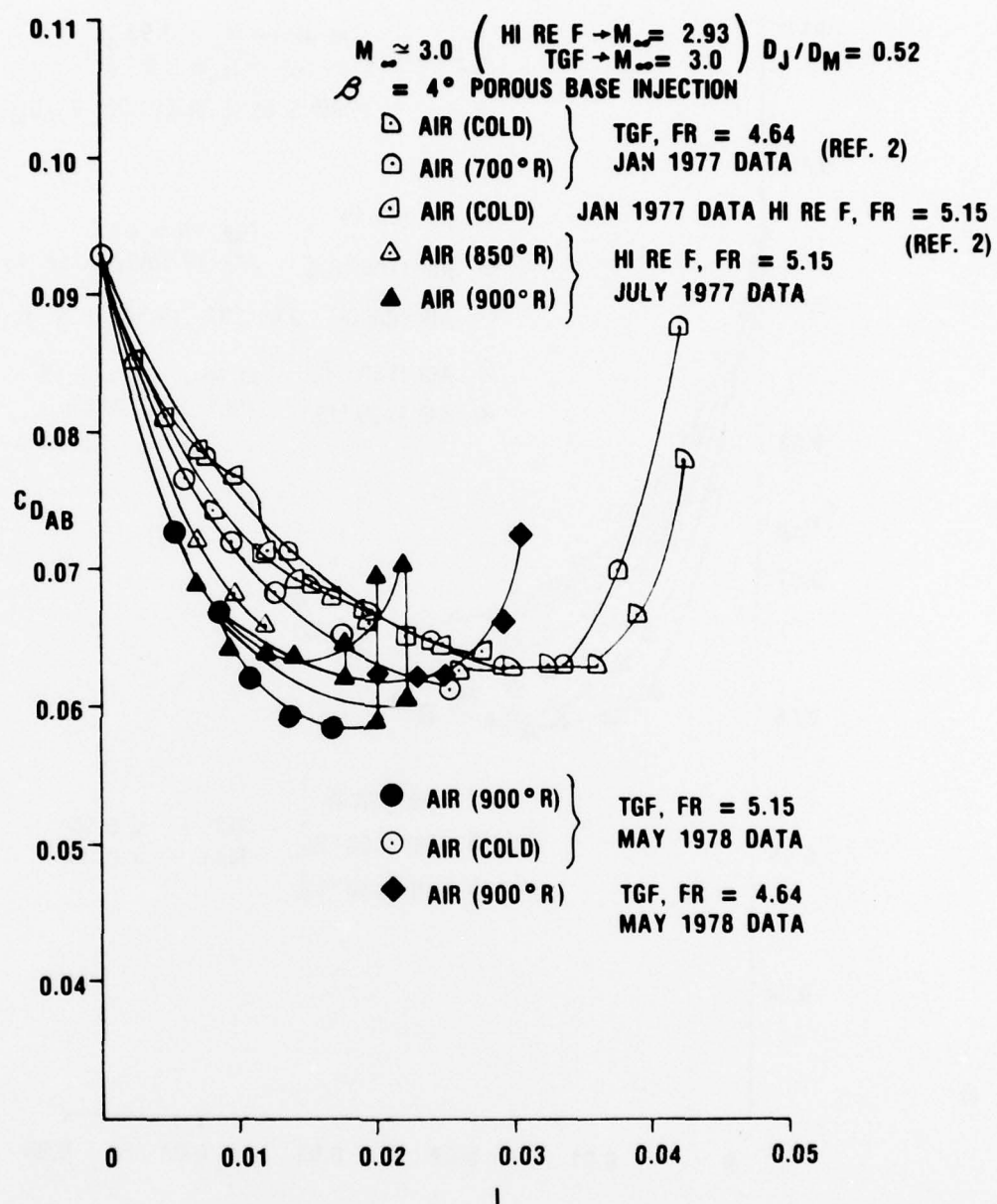
b. I=0.00475, Tg=900°R

c. I=0.006, Tg=905°R

Figure 10. Schlieren Photographs Showing Afterbody Flow Field Changes Due to the Increase of Base Injection Rates of Helium; β=7°

Figure 11.   Comparison of Afterbody Drag Coefficients Obtained With
Hot and Cold Injection
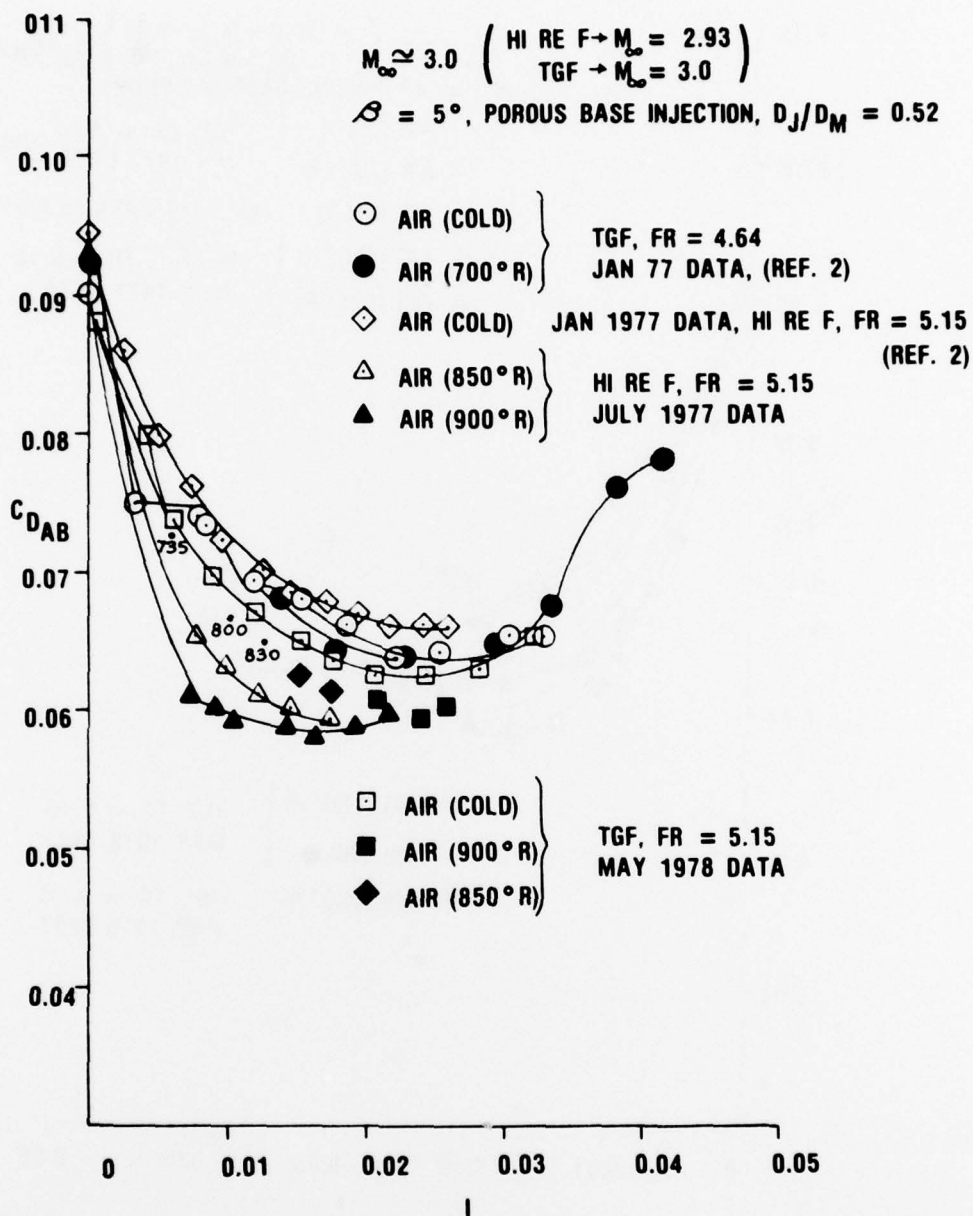
Figure 12.   Comparison of Afterbody Drag Coefficients Obtained With Hot
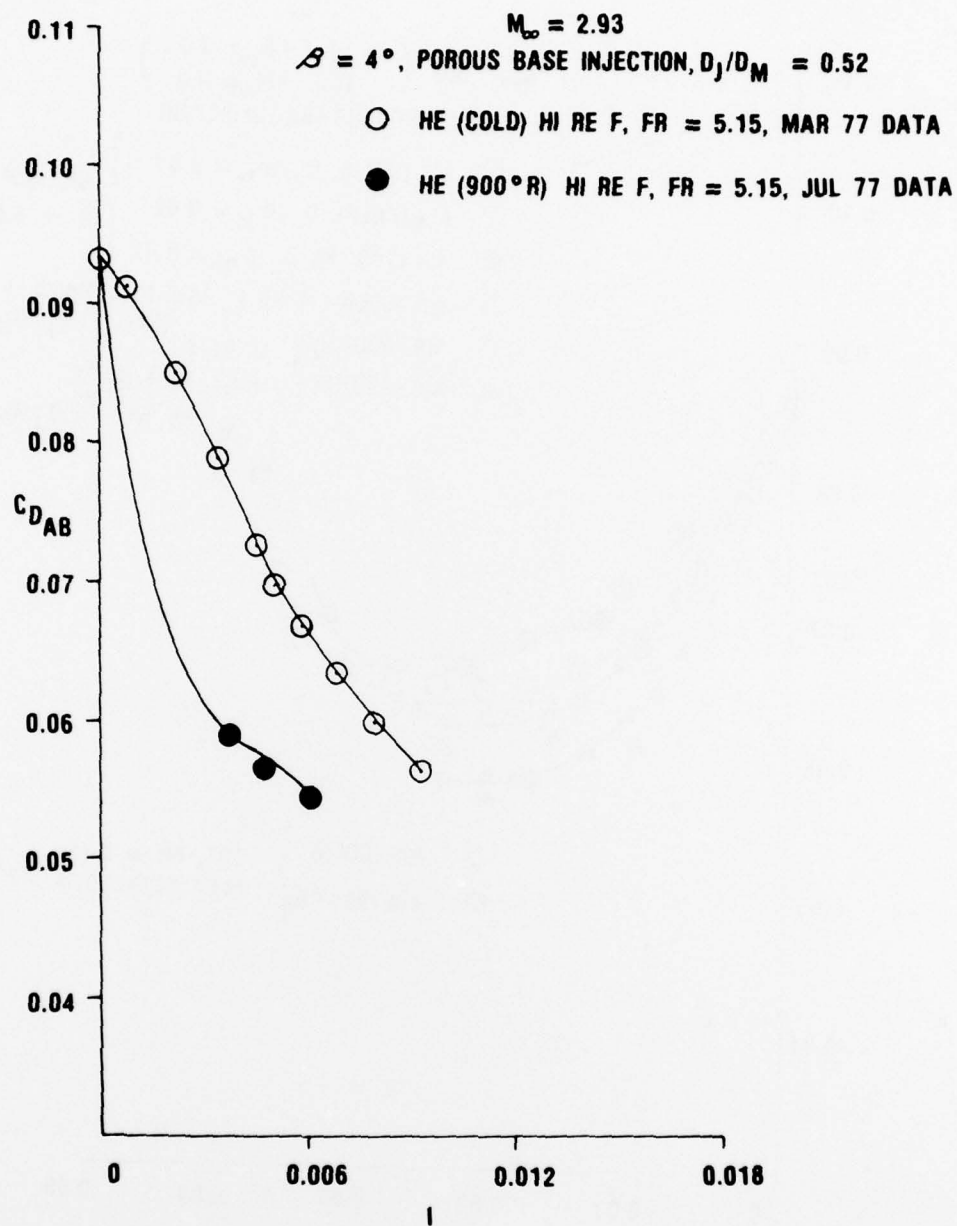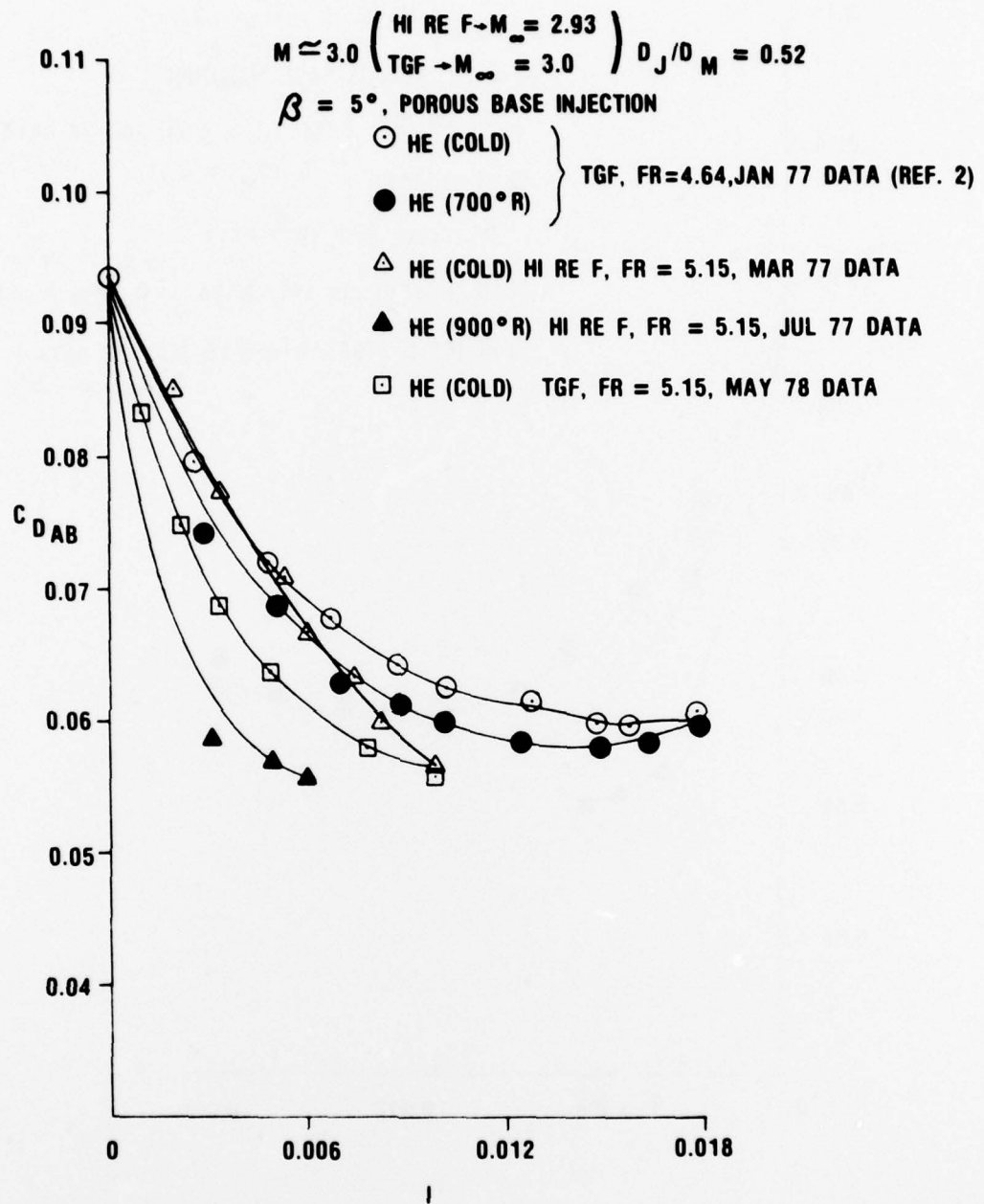and Cold Injection
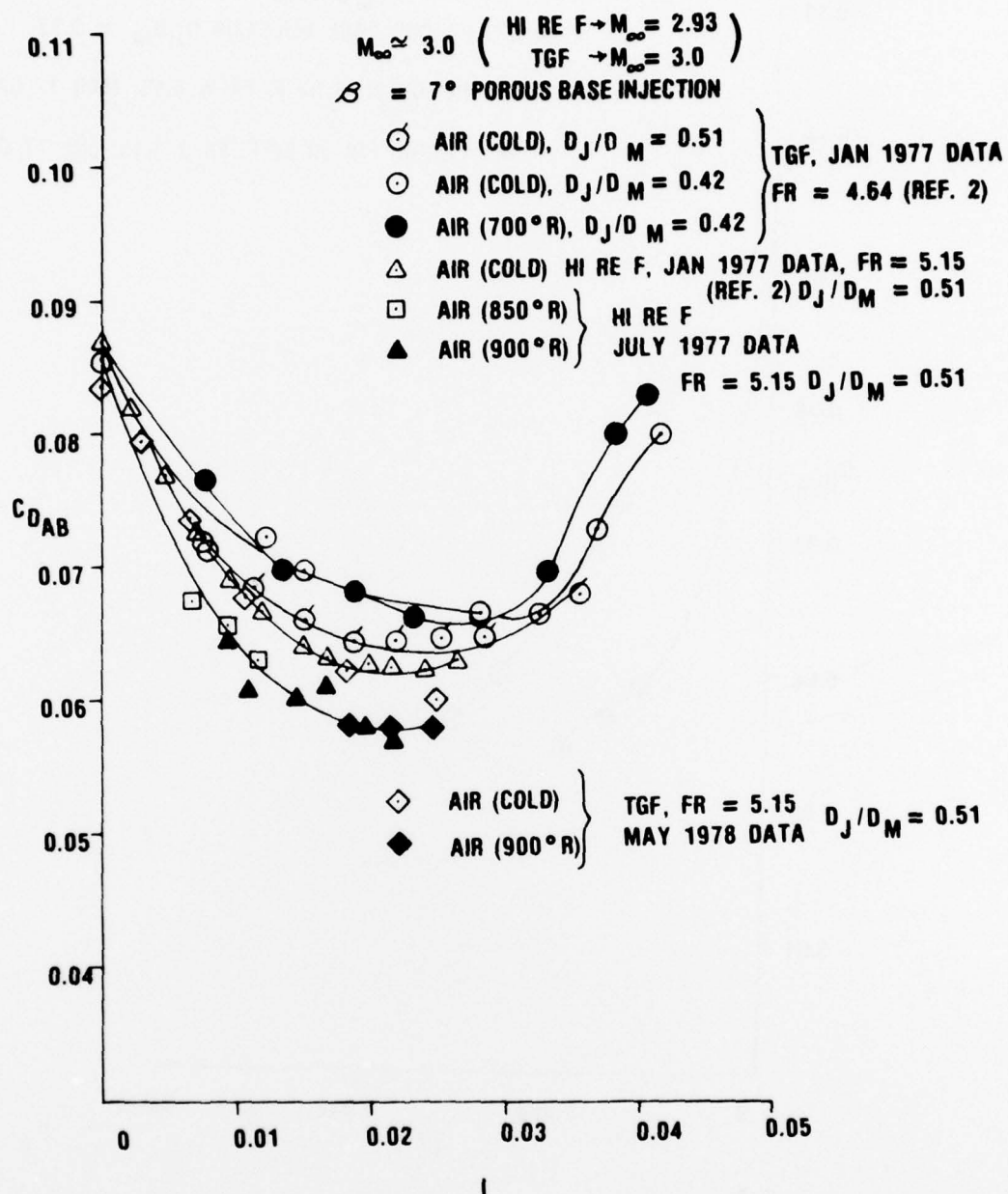
Figure 13. Comparison of Afterbody Drag Coefficients Obtained With Hot and Cold Injection

23

Figure 14. Comparison of Afterbody Drag Coefficients Obtained With Hot and Cold Injection

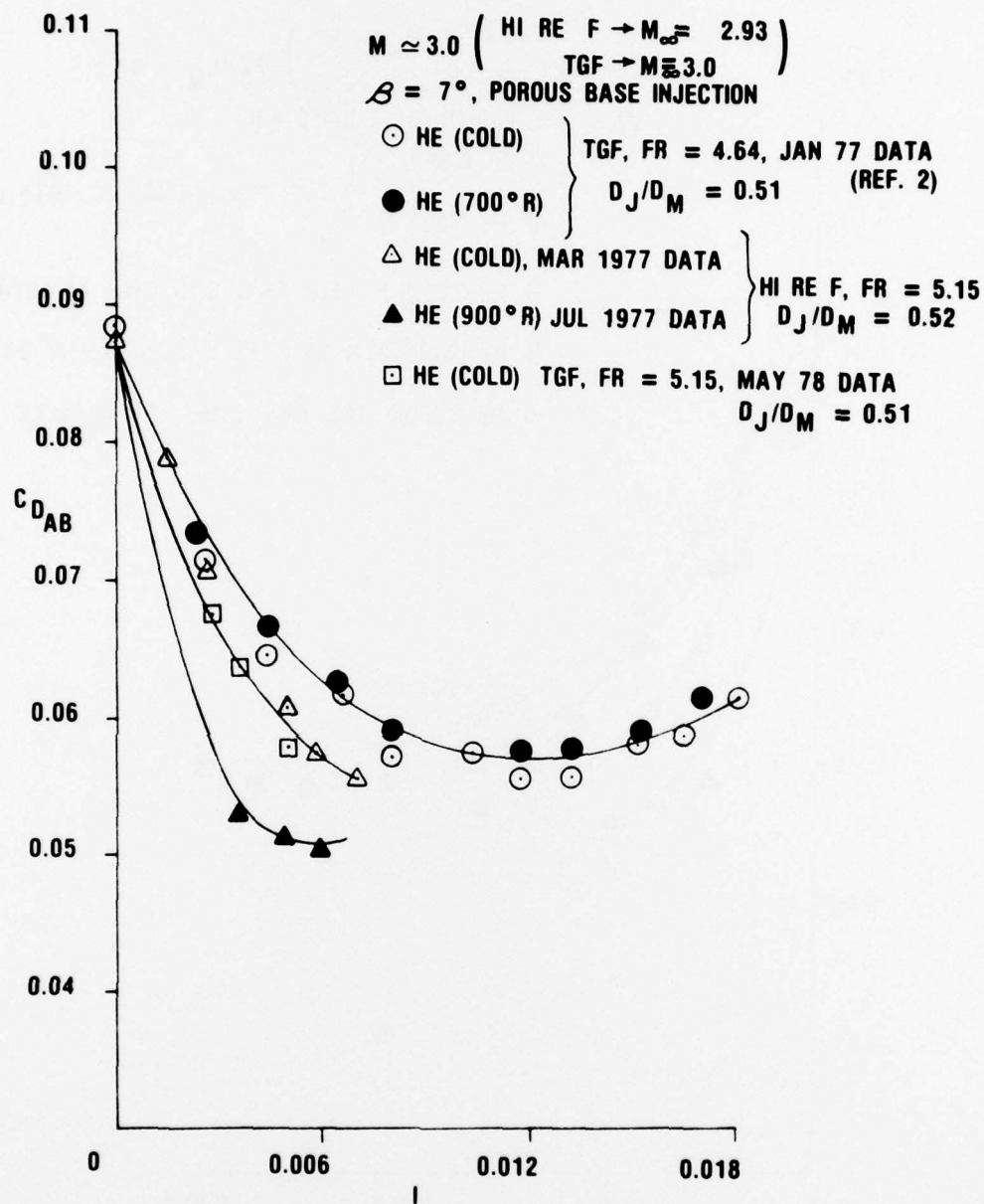Figure 15. Comparison of Afterbody Drag Coefficients Obtained With Hot and Cold Injection

Figure 16. Comparison of Afterbody Drag Coefficients Obtained With Hot and Cold Injection
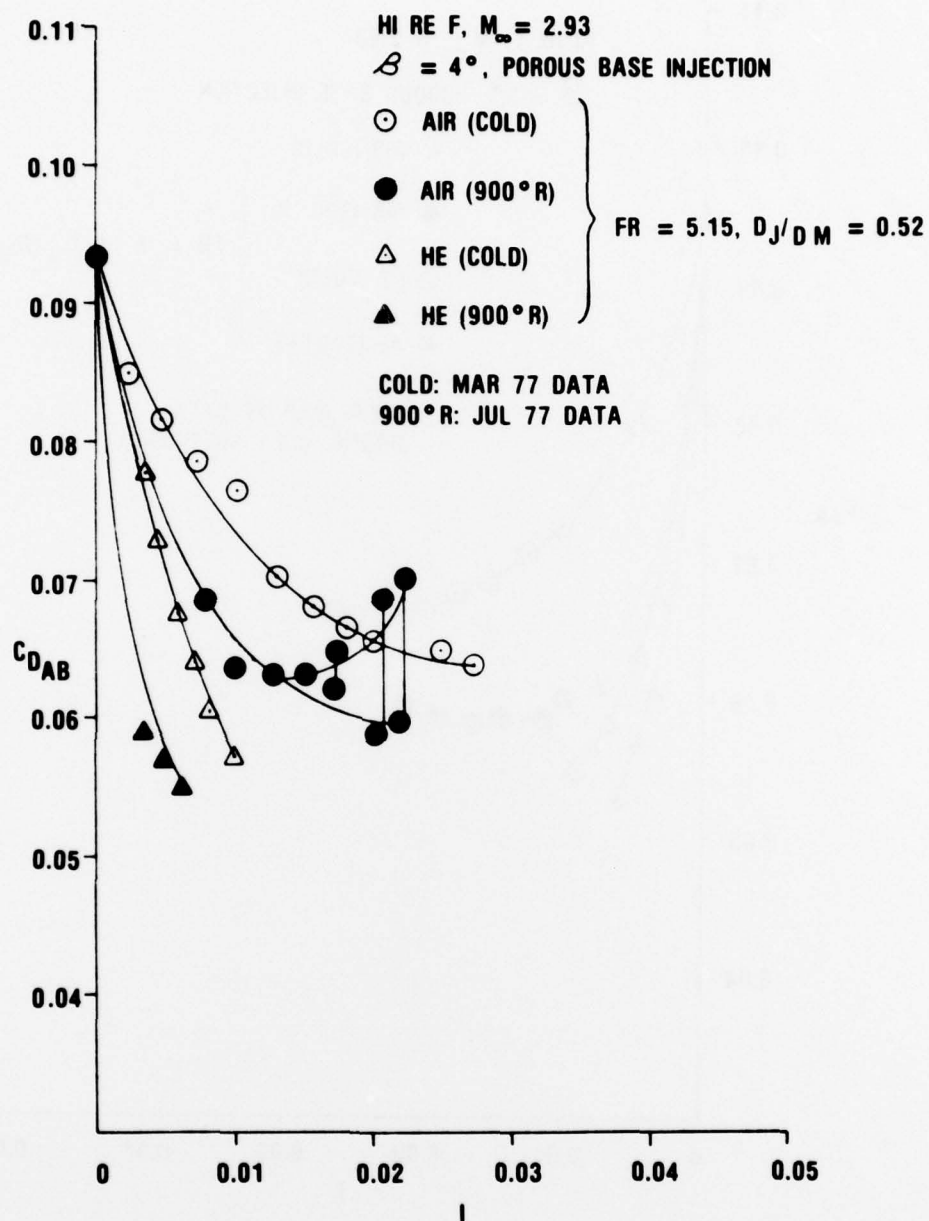
Figure 17. Afterbody Drag Coefficients Versus Injection Rate For
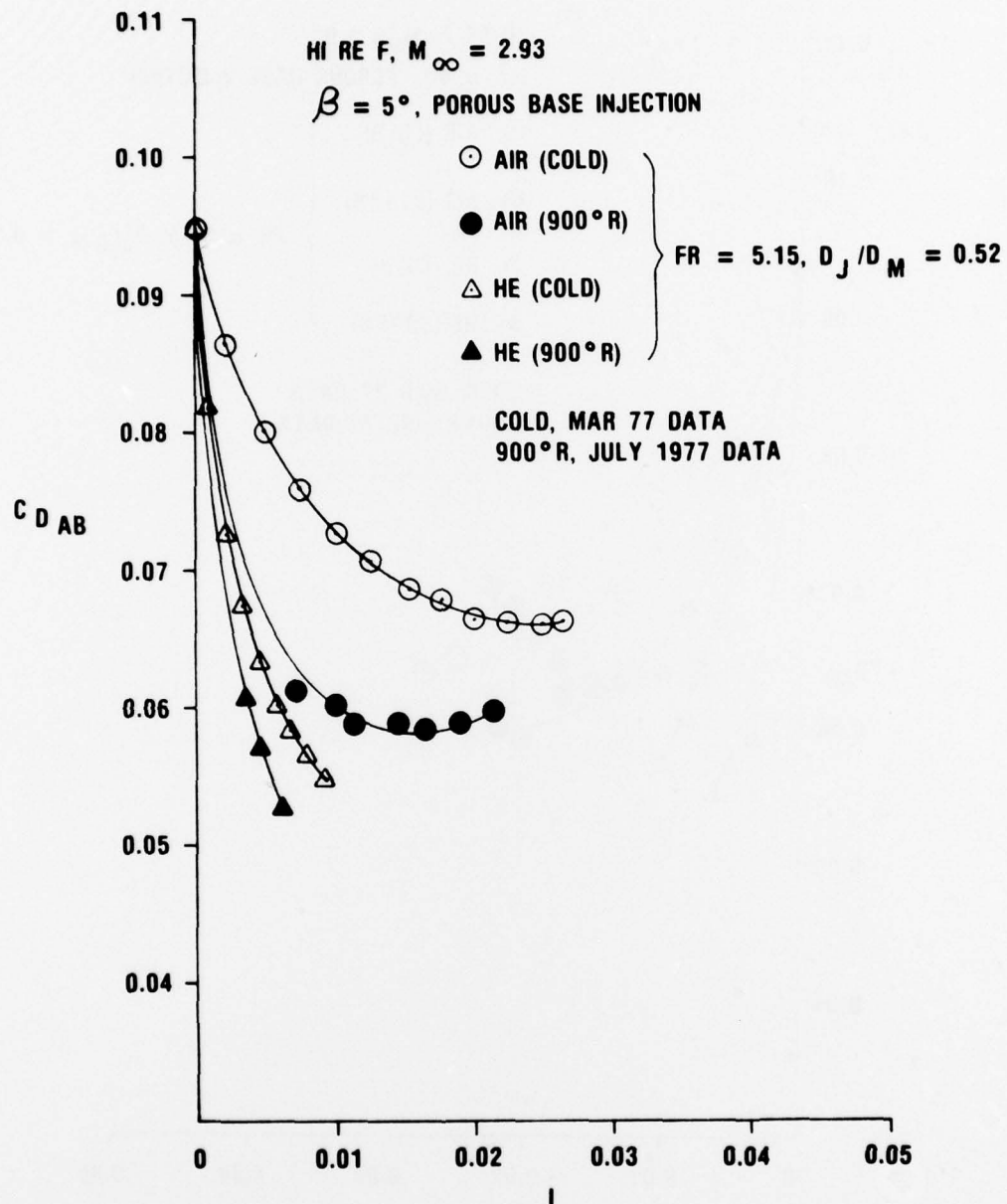Cold and Hot Air and Helium

Figure 18. Afterbody Drag Coefficients Versus Injection Rate for
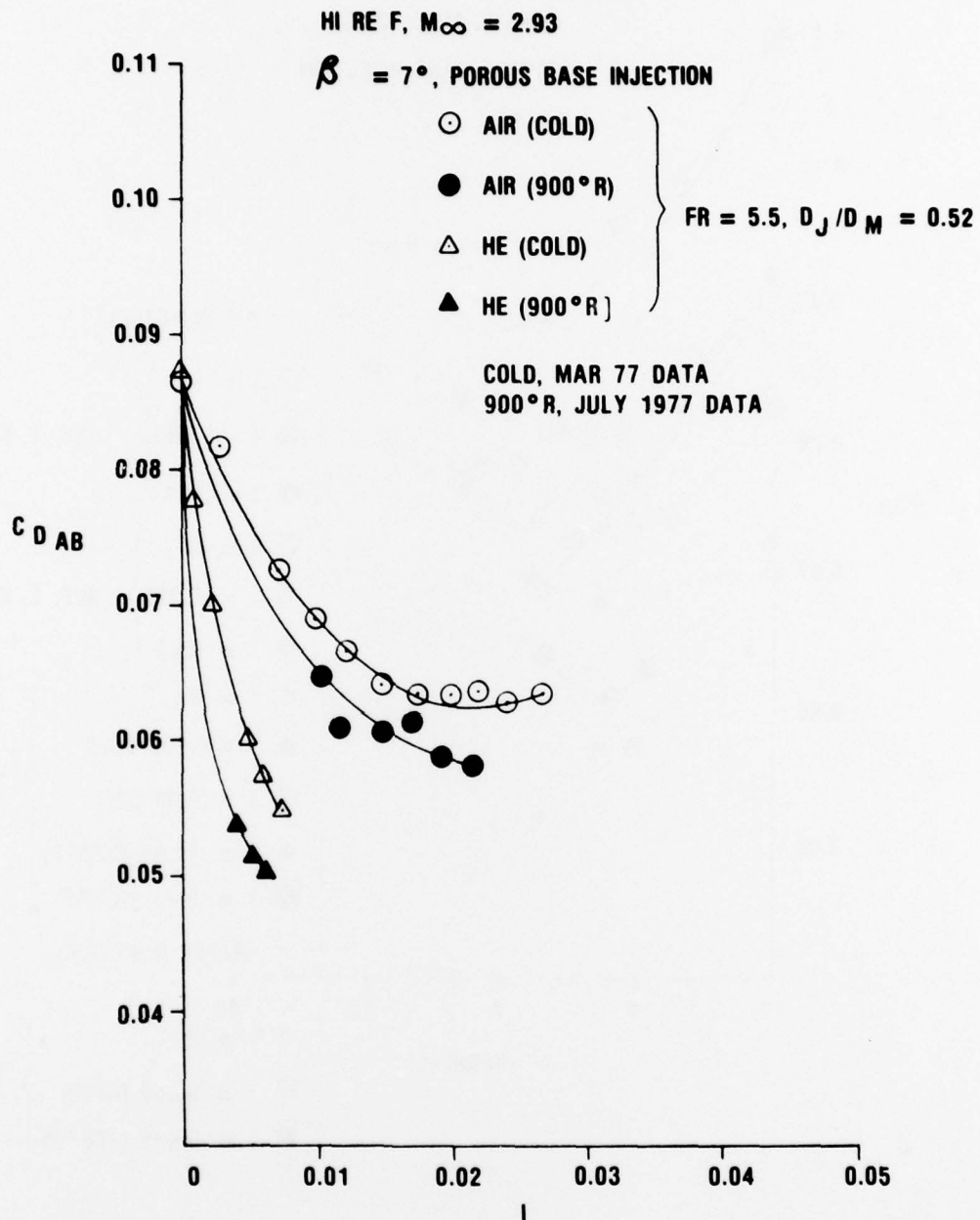Cold and Hot Air and Helium

28

Figure 19. Afterbody Drag Coefficients Versus Injection Rate for Cold and Hot Air and Helium
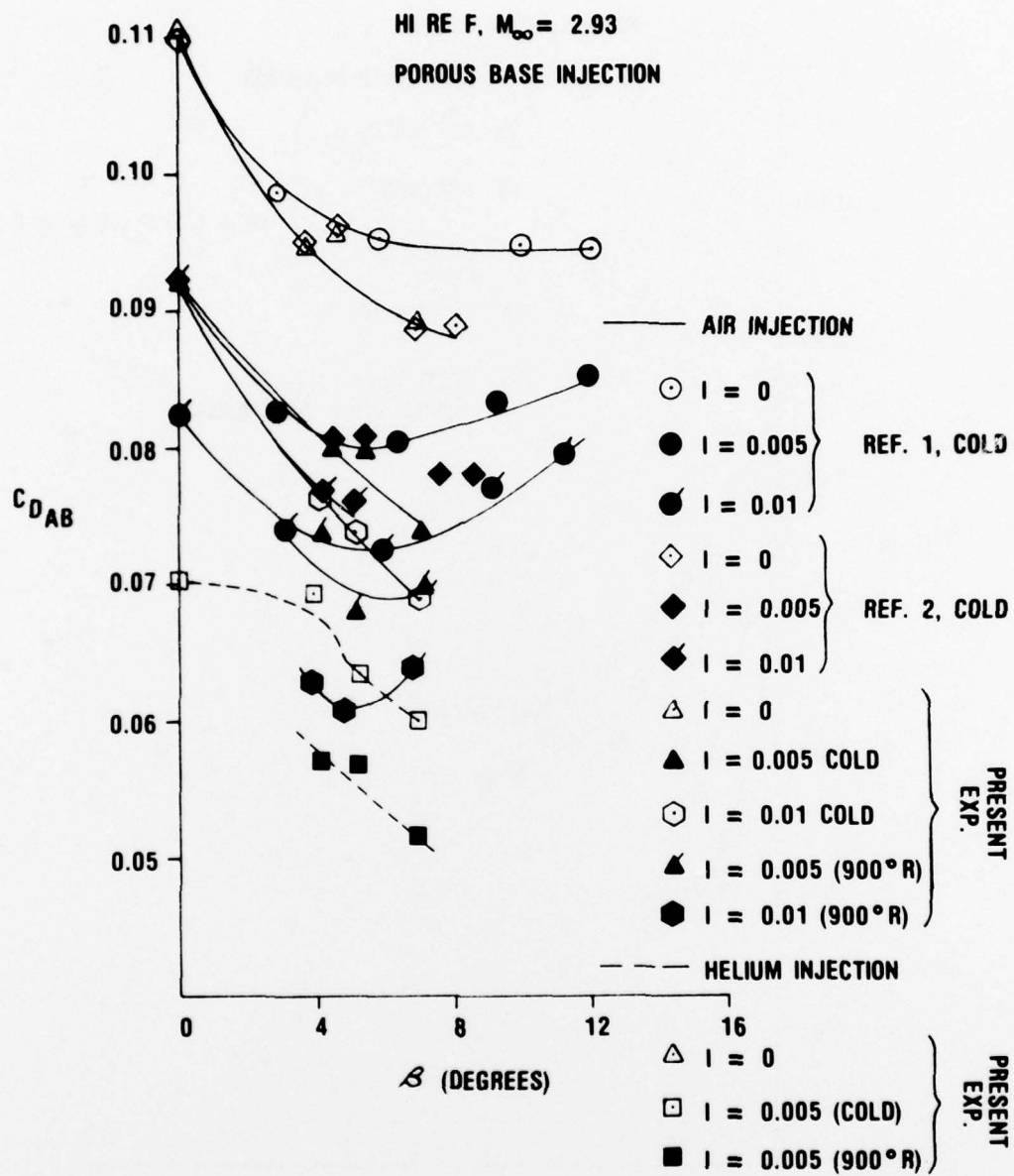
Figure 20.   Afterbody Drag Coefficients Versus Boattail Angle for
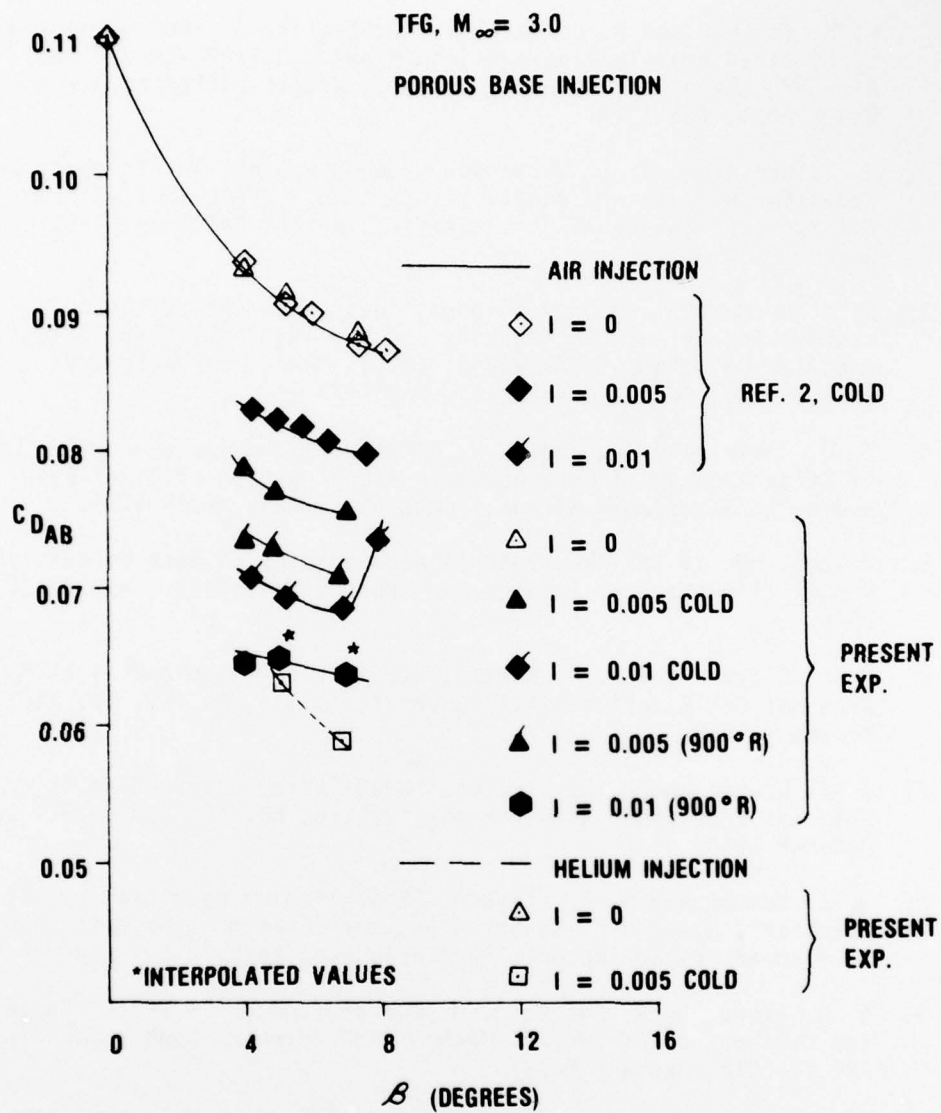Different Injection Rates

Figure 21. Afterbody Drag Coefficients Versus Boattail Angle for
Different Injection Rates

REFERENCES

1. L. M. Freeman and R. H. Korkegi, "Projectile Aft-Body Drag Reduction by Combined Boat-Tailing and Base Blowing," AFAPL-TR-75-112, Air Force Aero Propulsion Laboratory, Wright-Patterson Air Force Base, Ohio, Feb 1976.

2. W. Calarese and R. E. Walterick, "GAU-8 Projectile Afterbody Drag Reduction by Base and Boattail Injection," AFFDL TM-77-27-FXM, Air Force Flight Dynamics Laboratory, Wright-Patterson AFB, Ohio, March 1977.

3. S. N. B. Murthy and J. R. Osborn, "Base Flow Data With and Without Injection: Bibliography and Semi-Rational Correlations," Contract No. DAAD 05-72-C-0342, (BRL), School of Mechanical Engineering, Purdue University, May 1973.

4. E. M. Cortright, Jr. and A. H. Schroeder, "Preliminary Investigation of Effectiveness of Base Bleed in Reducing Drag of Blunt-Base Bodies in Supersonic Stream," NACA RM E51A26, March 1951.

5. Proceedings of the "Workshop of Aerodynamics of Base Combustion" School of Mechanical Engineering, Purdue University, May 29-30 1974.

6. W. A. Clayden and J. E. Bowman, "Cylindrical Afterbodies at $M_\infty = 2$ With Hot Gas Ejection," AIAA Journal, Vol. 6, No. 12, pp. 2429-2430, December 1968.

7. J. E. Bowman and W. A. Clayden, "Boat-Tailed Afterbodies at $M_\infty = 2$ With Gas Ejection," AIAA Journal, Vol. 6, No. 10, pp. 2029 - 2030, October 1968.

8. J. E. Bowman and W. A. Clayden, "Reduction of Base Drag by Gas Ejection", R.A.R.D.E. Report 4/69, Royal Armament Research And Development Establishment, Fort Halstead, Kent, U.K., December 1969.

9. A. W. Flore, D. G. Moore, D. H. Murray, and J. E. West, "Design and Calibration of the ARL Mach 3 High Reynolds Number Facility," ARL TR-0012, January 1975.

10. H. L. White, "Trisonic Gasdynamic Facility User Manual," AFFDL-TM-73-82-FXM, Air Force Flight Dynamics Laboratory, Wright-Patterson AFB, Ohio, June 1973.